Computers, Materials & Continua
DOI: 10.32604/cmc.2022.030793
Article

Throughput Enhancement for NOMA Systems Using Intelligent Reflecting Surfaces

Raed Alhamad[1,*] and Hatem Boujemaa[2]

[1]Information Technology Department, Saudi Electronic University, Riaydh, Saudi Arabia
[2]UCAR-SUPCOM-COSIM, Ariana, 2083, Tunisia
*Corresponding Author: Raed Alhamad. Email: ralhamad@seu.edu.sa
Received: 01 April 2022; Accepted: 29 May 2022

Abstract: In this article, we optimize the powers associated to Non Orthogonal Multiple Access (NOMA) users, sensing and harvesting duration for Cognitive Radio Networks (CRN). The secondary source harvests energy from node A signal. Then, it senses the channel to detect primary source. Then, the secondary source transmits a signal that is reflected by Intelligent Reflecting Surfaces (IRS) so that all reflections have a zero phase at any user. A set Ii of reflectors are associated to user Ui. The use of M = Mi = 512, 256, 128, 64, 32, 16, 8 reflectors per user offers 45, 42, 39, 36, 33, 30, 27 dB gain *vs.* the absence of IRS. We also suggest the use of IRS in energy harvesting. The use $P = 8$ reflectors for energy harvesting and M = Mi = 8 reflectors per user for data communications offers 7 and 38 dB gain *vs*. one IRS M = Mi = 8 and the absence of IRS. The use of $P = 16$ reflectors for energy harvesting and M = Mi = 8 reflectors per user for data communications offers 9 and 42 dB gain *vs*. one IRS M = Mi = 8 and the absence of IRS.

Keywords: CRN; NOMA; spectrum sensing; energy harvesting; throughput maximization

1 Introduction

IRS are used to maximize the throughput of wireless systems as all reflections have a zero phase at the destination [1–5]. The phase of the p-th reflector is computed using the phase of channel gains of the links between the source and IRS as well as that of the link between IRS and the destination [6–8]. IRS have been used in NOMA systems where a set Ii of reflectors are associated to user Ui [9]. The results of [9] are not valid for CRN as a single network was studied without energy harvesting and spectrum sensing. IRS have been deployed to maximize the throughput of millimeter wave and optical systems [10–12]. The asymptotic behavior of wireless systems using IRS was derived in [13–16]. Experimental results of IRS were provided in [17–19]. Continuous reserve skyline queries in Wireless Sensor Networks (WSN) was proposed in [20]. A self adaptive multivariate data compression with error bound was proposed in [21] for WSN. A particle swarm optimization was used in [22] to enhance the coverage in WSN. A hamilton loop based data collection algorithm can also be used in WSN [23].

Optimal coverage using multipath scheduling scheme was suggested in [24]. In [25], asynchronous clustering has been combined with data gathering scheme for WSN. In [26], the authors proposed a power efficient gathering technique in sensor information systems. A minimal connected dominant set was optimized in [27] to enhance WSN routing protocol. Coverage and network connectivity were optimized in [28] for mobile sensor networks.

In this article, we optimize NOMA powers, sensing and harvesting durations to maximize the throughput. After energy harvesting from node A signal, secondary source SS senses the channel to detect primary activity. When no activity is detected, the secondary source transmits a signal that is reflected by IRS so that all reflections have a zero phase at any NOMA user. A set Ii of reflectors are associated to user Ui. The use of M = Mi = 512, 256, 128, 64, 32, 16, 8 reflectors per user offers 45, 42, 39, 36, 33, 30, 27 dB gain *vs*. wireless systems without IRS [29]. We also improve the energy harvesting process using IRS between A and SS. In this case, energy harvesting uses reflected signals with zero phase at SS. A second IRS contains different sets of optimized reflectors to deliver reflections with a zero phase at any user Ui. The use $P = 8$ reflectors for energy harvesting and M = Mi = 8 reflectors per user for data communications offers 7 and 38 dB gain *vs*. one IRS M = Mi = 8 and the without IRS [29]. Using $P = 16$ reflectors for energy harvesting and M = Mi = 8 reflectors per user for data communications offers 9 and 42 dB gain *vs*. one IRS M = Mi = 8 and the absence of IRS [29].

Next section optimizes the NOMA powers, sensing and harvesting durations. Section 3 improves the energy harvesting process using IRS. Section 4 gives some results and Section 5 concludes the paper.

2 Throughput Analysis with a Single IRS

2.1 System Model

In Fig. 1, there are a Primary Destination and Source PD and PS, a Secondary Source SS and K secondary users, node A and IRS used as a reflector. In the first phase, energy harvesting is performed at SS over μ T s using the signal of A where T is frame length in s and $0 < \mu < 1$. Then, SS senses the channel over $(1-\mu)\zeta$T s using samples of the received signal from PS. When PS is inactive, SS broadcasts a signal to K NOMA users over $(1-\mu)(1-\zeta)$T s. The aim of the paper is to optimize the powers of NOMA users as well as sensing and harvesting durations throughput the parameters μ and ζ to maximize the total throughput while using intelligent reflecting surfaces.

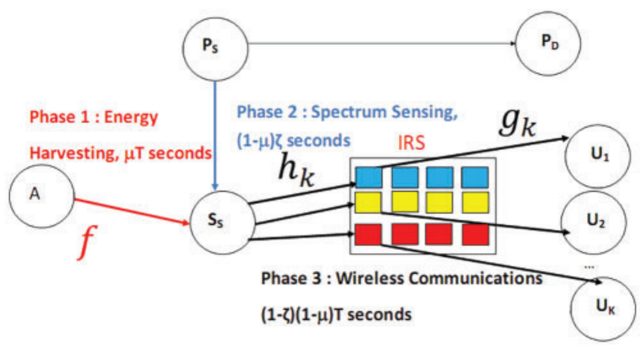

Figure 1: Network model

2.2 Energy Harvesting Without IRS

The harvested energy is given by

$$E = \beta\mu TP_A|f|^2 = \beta\mu L_0 E_A|f|^2 \tag{1}$$

where β is an efficiency coefficient, $P_A = E_A/Ts$ is the power of A, Ts is the symbol duration, f is channel gain from A to SS, $L_0 = T/Ts$. We can write $E(|f|^2) = 1/dAS_S{}^{ple}$ where d_{XY} is the distance from X to Y and ple is the path loss exponent.

The symbol energy of S_S is computed as:

$$E_{SS} = \frac{E}{L_0(1-\mu)(1-\zeta)} = \frac{\beta\mu E_A|f|^2}{(1-\mu)(1-\zeta)} \tag{2}$$

In Fig. 1, the users are ranked as follows: U1 is the strong user, Ui is the i-th strong user and UK is the weak user. The transmitted NOMA symbol by S_S is equal to

$$s = \sqrt{E_{SS}}\sum_{i=1}^{K} PO_i s_i, \tag{3}$$

si is the symbol of user Ui and $0 < PO_i < 1$ is the power allocated to Ui such that $0 < PO_1 < PO_2 < \cdots < PO_K < 1$ and $\sum_{i=1}^{K} PO_i = 1$.

Let hp be the channel from S_S to p-th IRS reflector. Let gp be the channel from p-th IRS reflector to Ui. Ii is a set of reflectors associated to Ui and contains Mi = |Ii| reflectors. We have: $E(|hp|^2) = 1/dSSIRS^{ple}$. Furthermore, we have $E(|gp|^2) = 1/dIRSUi^{ple}$.

We have hp = apexp(−jbp) where ap = |hp|. $E(aq) = \Gamma(m+0.5)/[\Gamma(m)\sqrt{Md_{SSIRS}^{ple}}]$ and $E(aq^2) = 1/d_{SSIRS}{}^{ple}$ [30]. We have gp = cpexp(−jep) where cp = |gp| and ep is the phase of gp. We have $E(cq) = \Gamma(m+0.5)/[\Gamma(m)\sqrt{Md_{IRSUi}^{ple}}]$ and $E(aq^2) = 1/d_{IRSUi}{}^{ple}$ [30].

The phase of p-th reflector is equal to [1]

$$\varphi p = bp + ep. \tag{4}$$

The received signal at Ui is given by

$$r_i = s\sum_{i\in Ii} h_p g_p exp\left(-j\varphi_p\right) + n_i, \tag{5}$$

where ni is a Gaussian r.v. of variance N0.

Eq. (3) gives

$$r_i = s\sum_{i\in Ii} a_p c_p + n_i = \sqrt{Y_i}s + n_i, \tag{6}$$

where

$$Y_i = E_{SS}F_i^2 \tag{7}$$

$$F_i = \sum_{i\in Ii} a_p c_p, \tag{8}$$

In (6), we notice that the phase shifts of reflectors given in (4) have been chosen so that all reflections have a zero phase at user Ui.

Using (2), we deduce

$$Y_i = F_i^2 \frac{\beta \mu E_A |f|^2}{(1-\mu)(1-\zeta)} \tag{9}$$

Fi follows a Gaussian distribution with mean mFi = Mi $\Gamma(m+0.5)^2/[\Gamma(m)^2 d_{SSIRS}^{ple/2} d_{IRSUi}^{ple/2}]$ and variance $\sigma Fi^2 = M/[d_{SSIRS}^{ple} d_{IRSUi}^{ple}][1-\Gamma(m+0.5)^4/Mi^2/\Gamma(m)^4]$. Therefore, Fi^2 has a non-central-chisquare distribution with degree of freedom one. For Rayleigh channels, $|f|^2$ has also a central-chisquare distribution with degrees of freedom 2 m. Therefore, Yi is the product of a non-central and a central chisquare random variables and we have [31]

$$P_{Yi}(x) = P(Yi < x) = \frac{e^{-0.5\frac{m_X^2}{\sigma_X^2}}}{\Gamma(m)} \sum_{q=0}^{+\infty} \frac{\left(\frac{m_X^2}{\sigma_X^2}\right)^q}{2^q \Gamma(q+0.5)} G_{1,3}^{2,1}\left(\frac{N_0(1-)(1-\zeta)\, xmd_{ASS}^{ple}}{2\beta\mu E_A} |_{q+0.5, m, 0}^{1}\right), \tag{10}$$

where $G_{n,m}^{p,l}(x)$ is the Meijer G-function.

We deduce

$$r_i = \sqrt{Y_i} \sum_{j=1}^{K} PO_j s_j, + + n_i \tag{11}$$

2.3 Signal to Interference Plus Noise Ratio (SINR) and Throughput Analysis

Ui performs Successive Interference Cancelation (SIC) and detects first s_K since $PO_K > PO_i$. The corresponding SINR is

$$\Gamma^{i\to K} = \frac{Y_i PO_K}{N_0 + Y_i \sum_{p=1}^{K-1} PO_p} \tag{12}$$

The contribution of the detected symbol sK is removed and Ui estimates s_{K-1} with the following SINR

$$\Gamma^{i\to K-1} = \frac{Y_i PO_{K-1}}{N_0 + Y_i \sum_{p=1}^{K-2} PO_p} \tag{13}$$

The process is continued by detecting sl with SINR

$$\Gamma^{i\to l} = \frac{Y_i PO_l}{N_0 + Y_i \sum_{p=1}^{l-1} PO_p} \tag{14}$$

The probability of an outage event at Ui is computed as

$$Pout, i(x) = 1 - P(\Gamma^{i\to i} > x, \ldots, \Gamma^{\, i\to K} > x)$$

$$= P_{Yi}\left(max_{i\le l\le K} \frac{N_0 x}{PO_l - x\sum_{p=1}^{l-1} PO_p}\right) \tag{15}$$

where $P_{Yi}(y)$ is provided in (10). In Eq. (15) $\Gamma^{i\to l}$>x corresponds to $Yi > \frac{N_0 x}{PO_l - x\sum_{p=1}^{l-1} PO_p}$. Therefore, Yi should be larger than the maximum of these values for l = i, . . . , K which is $max_{i\le l\le K} \frac{N_0 x}{PO_l - x\sum_{p=1}^{l-1} PO_p}$

The Packet Error Probability (PEP) at Ui is equal to [32]

$$\mathrm{PEPi}(\mathrm{PO1}, \mathrm{PO2}, \ldots, \mathrm{POK}, \mu, \zeta) < \mathrm{P}_{\mathrm{outage}}(\mathrm{T}_0) \tag{16}$$

where T_0 is defined as [12]

$$T_0 = \int_0^{+\infty} 1 - \left[1 - 2\left(1 - \frac{1}{\sqrt{Q}}\right) erfc\left(\sqrt{\frac{3ulog_2(Q)}{2Q-2}}\right)\right]^{PL} du, \tag{17}$$

where PL is packet length.

The total throughput is equal to

$$Thr(PO_1, \ldots, PO_K, \mu, \zeta) = (1-\mu)(1-\zeta)\, log2(Q)\, Pidle(1-Pf)$$

$$\times \sum_{i=1}^{K} [1 - PEP_i(PO_1, \ldots, PO_K, \mu, \zeta)] \tag{18}$$

where Pf is the probability of a false alarm

$$P_f = \frac{\Gamma(\lfloor(1-\mu)\zeta L0\rfloor, T1/2)}{\Gamma(\lfloor(1-\mu)\zeta L0\rfloor)}, \tag{19}$$

where T1 is the energy detector threshold

The powers of NOMA users, sensing and harvesting durations μ and ζ are optimized as follows:

$$(\mathrm{PO_1}^{\mathrm{opt}}, \ldots, \mathrm{PO_K}^{\mathrm{opt}}, \mu^{\mathrm{opt}}, \zeta^{\mathrm{opt}}) = \mathrm{argmaxThr}(\mathrm{PO_1}, \ldots, \mathrm{PO_K}, \mu, \zeta) \tag{20}$$

3 IRS to Enhance the Energy Harvesting Process

3.1 System Model

Fig. 2 shows that data transmission can use two IRS. IRS_1 contains P reflectors between A to SS to enhance the energy harvesting process. IRS_2 is between SS and users Ui with Mi reflectors to improve the throughput.

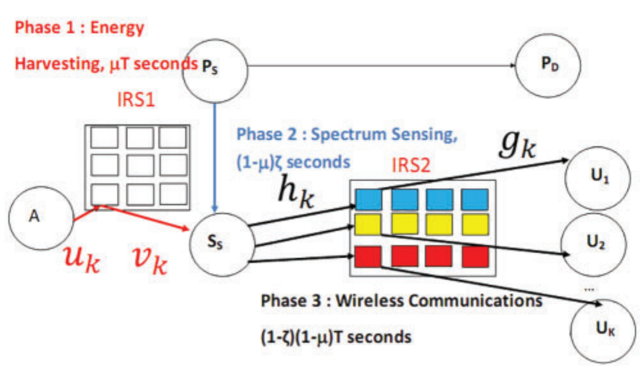

Figure 2: IRS used in energy harvesting

3.2 Energy Harvesting Using IRS

When energy harvesting uses IRS, we have

$$\mathrm{E} = \beta\mu \mathrm{L_0 E_A C^2}, \tag{21}$$

where

$$Z = \sum_{p=1}^{P} \delta_p \eta_p \tag{22}$$

where δp = |up|, up is the channel from A to p-th IRS1 reflector and ηp = |vp|, vp is the channel from p-th reflector of IRS1 to SS.

The mean and variance of C are equal to

$$m_C = \frac{P\Gamma(m+0.5)^2}{m\Gamma(m)^2 d_{AIRS1}^{ple/2} d_{IRS1SS}^{PLE/2}} \tag{23}$$

$$\sigma_C^2 = \frac{P}{d_{AIRS1}^{ple/2} d_{IRS1SS}^{ple/2}}[1 - \frac{\Gamma(m+0.5)^4}{{M_1}^2\Gamma(m)^4}] \tag{24}$$

We deduce

$$E_{SS} = \frac{E}{L_0(1-\mu)(1-\zeta)} = \frac{\beta\mu E_A C^2}{(1-\mu)(1-\zeta)} \tag{25}$$

The variable Yi should be replaced by Zi written as

$$Y_i = F_i^2 \frac{\beta\mu E_A C^2}{(1-\mu)(1-\zeta)} \tag{26}$$

where Fi is defined in (8).

Zi is the product of two non central chisquare r.v. Therefore, we have [31]

$$P_{Z_i}(x) = e^{-0.5\frac{m_{Fi}^2}{\sigma_{Fi}^2}} e^{-0.5\frac{m_C^2}{\sigma_C^2}} \sum_{q=0}^{+\infty}\sum_{l=0}^{+\infty} \frac{\left(\frac{m_{Fi}^2}{\sigma_{Fi}^2}\right)^l \left(\frac{m_C^2}{\sigma_C^2}\right)^q}{2^{q+l}\Gamma(q+0.5)\Gamma(l+0.5)\, q!\, l!}$$
$$\times\ G_{1,3}^{2,1}\left(\frac{N_0(1-)(1-\zeta)\,xm}{\beta E_A 2}\Big|_{q+0.5,\, l+0.5,\, 0}^{1}\right), \tag{27}$$

4 Numerical Results

Fig. 3 depicts the total throughput for K = 2 users, QPSK modulation, m-fading figure m = 2, β = 0.5, T1 = 1, dASS = 1.1, dSSIRS = 1.2, dIRSU1 = 1.1, dIRSU2 = 1.5 and ple = 3. We notice that the use of M = Mi = 512, 256, 128, 64, 32, 16, 8 reflectors per user offers 45, 42, 39, 36, 33, 30, 27 dB gain *vs*. the absence of IRS [29]. Fig. 3 corresponds to optimal PO_i, μ and ζ.

Figs. 4 and 5 compares the total throughput for M = Mi = 8, 16 with optimal μ and ζ to (μ = 1/3, ζ = 1/2). We observe that optimal harvesting and sensing duration μ and ζ offers a better throughput than (μ = 1/3, ζ = 1/2), (μ = 1/3, optimal ζ) and (optimal μ, ζ = 1/2).

Fig. 6 shows the total throughput for K = 3 users and 16QAM modulation, m-fading figure m = 2, T1 = 1, d = 1, dSSIRS = 1.2, dIRSU1 = 1.1, dIRSU2 = 1.3, dIRSU3 = 1.5. M = Mi = 512, 256, 128, 64, 32, 16, 8 reflectors per user offers 47, 44, 41, 38, 35, 32, 29 dB gain *vs*. NOMA without IRS [29]. In Fig. 6, we used an optimal powers as well as optimal μ and ζ.

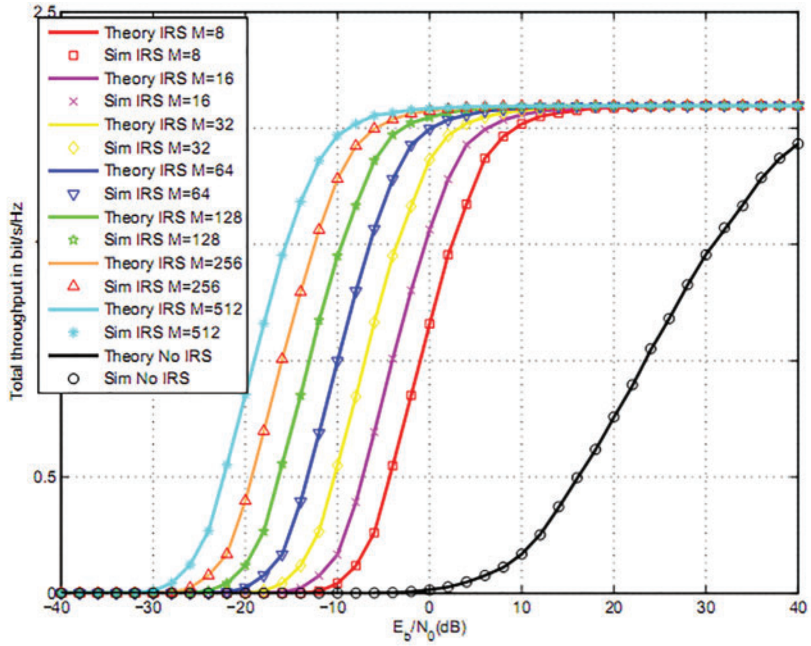

Figure 3: Total throughput for two users and QPSK

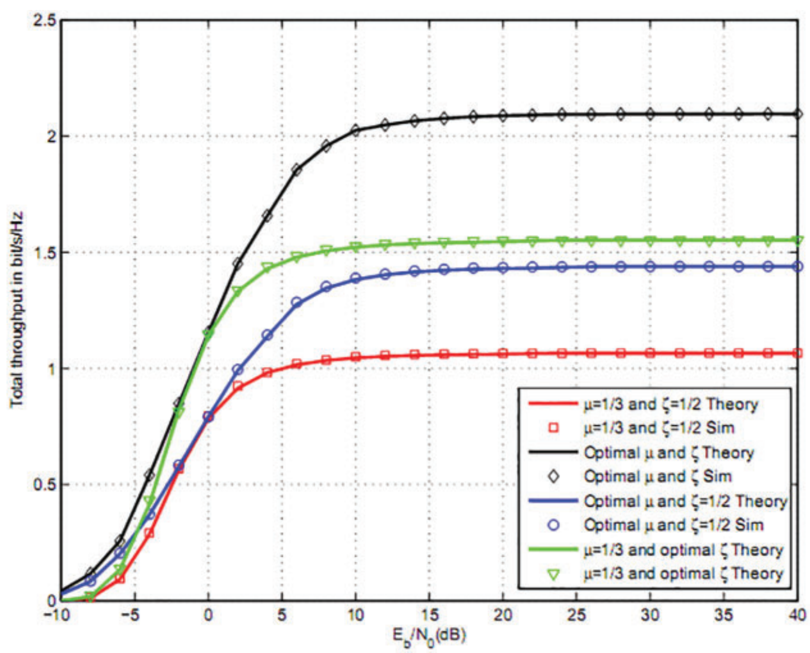

Figure 4: Total throughput for two users QPSK and M = 8

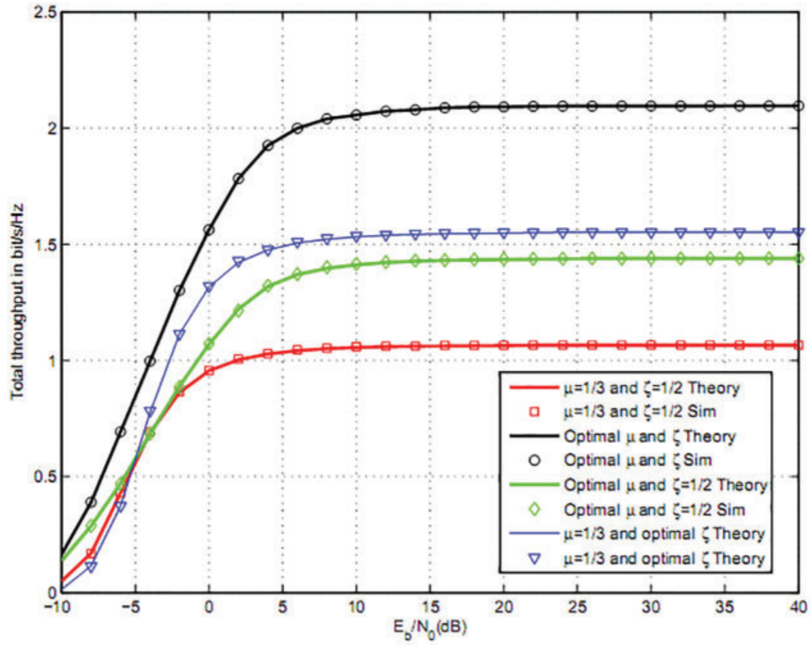

Figure 5: Total throughput for two users, QPSK and M = 16

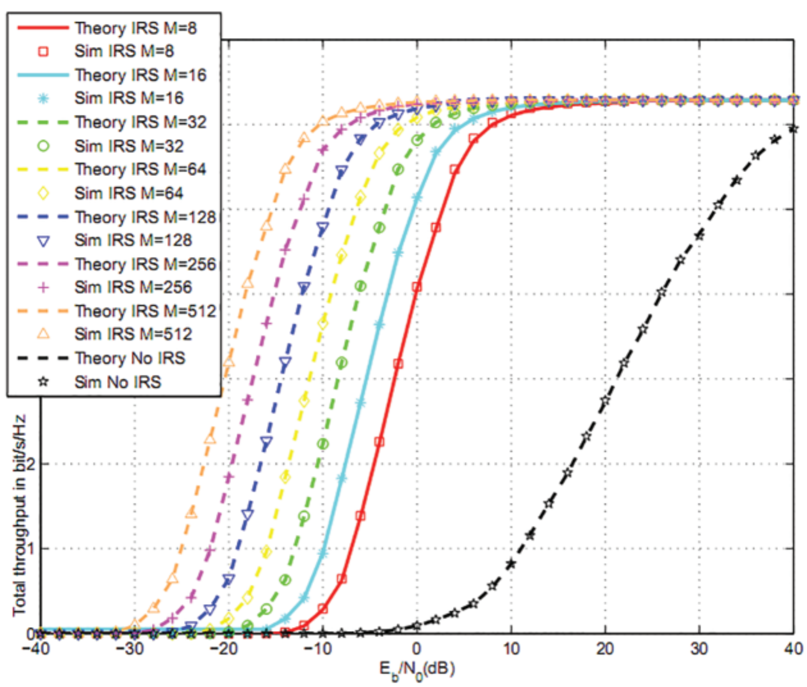

Figure 6: Total throughput for three users and 16QAM

Fig. 7 depicts the throughput for M = Mi = 16 reflectors per user. We optimized NOMA powers in Fig. 7. We observe that optimal sensing and harvesting durations ζ and μ offers a better throughput than (μ = 1/3, ζ = 1/2), (μ = 1/3, optimal ζ) and (optimal μ, ζ = 1/2).

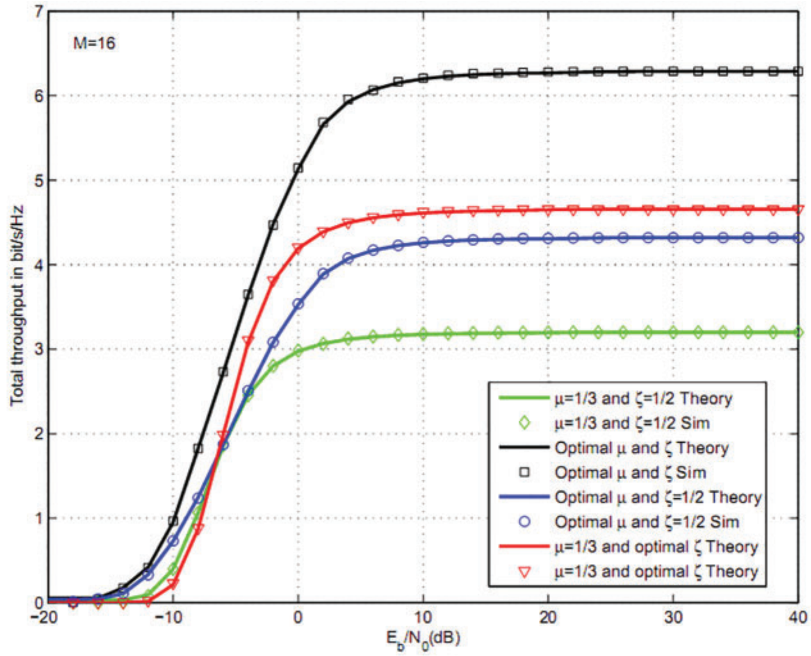

Figure 7: Total throughput for three users, 16QAM and M = 16

Fig. 8 shows the total throughput for the same parameters as Fig. 6. We have studied the effect of m-fading figure. For m = 3, we observe up to 8 and 2 dB gain *vs*. m = 1 and m = 2 that corresponds to Rayleigh channels.

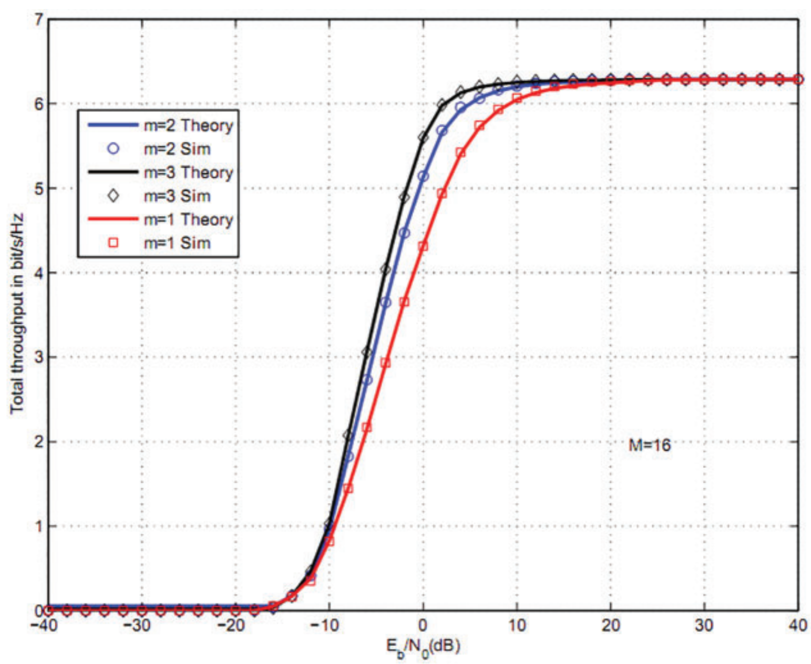

Figure 8: Total throughput for three users, 16QAM and M = 16

In Fig. 9, we plotted the total throughput for K = 3 users and 16QAM modulation. The parameters are the same as Fig. 6. We have plotted the throughput when a energy harvesting uses IRS. The parameters are dAIRS1 = 1.1 and dIRS1SS = 1.3. The use $P = 8$ reflectors for energy harvesting and M = Mi = 8 reflectors per user for data communications offers 7 and 38 dB gain *vs*. one IRS M = Mi = 8 and without IRS [29]. The use of $P = 16$ reflectors for energy harvesting and M = Mi = 8 reflectors per user for data communications offers 9 and 42 dB gain *vs*. one IRS M = Mi = 8 and without IRS [29].

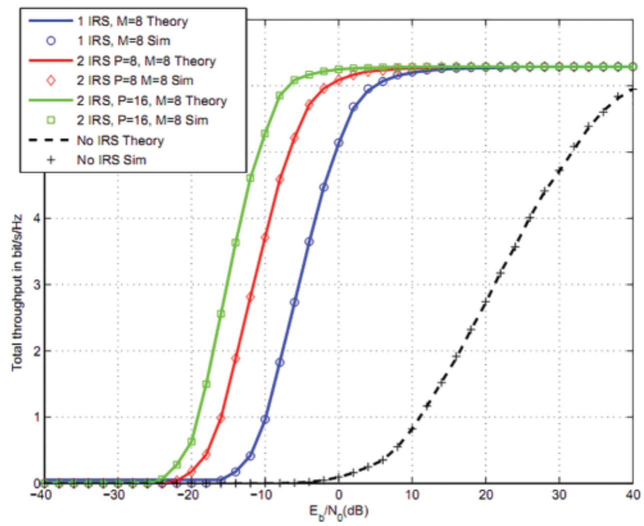

Figure 9: Total throughput using two IRS: three users, 16QAM

5 Conclusion

In this article, we optimized the powers of NOMA users, sensing and harvesting duration for CRN. Secondary source senses the channel over $(1-\mu)\zeta T$ s to detect primary activity. If no activity is detected, SS broadcasts a signal during $(1-\mu)(1-\zeta)T$ s to NOMA users. The signal is reflected by Intelligent Reflecting Surfaces (IRS) towards K users. A set Ii of reflectors is associated to user Ui. The use of M = Mi = 512, 256, 128, 64, 32, 16, 8 reflectors per user offers 45, 42, 39, 36, 33, 30, 27 dB gain *vs*. wireless systems without IRS [29]. We also suggest the use of IRS in energy harvesting. The use $P = 8$ reflectors for energy harvesting and M = Mi = 8 reflectors per user for data communications offers 7 and 38 dB gain *vs*. one IRS M = Mi = 8 and without IRS [29]. The use of $P = 16$ reflectors for energy harvesting and M = Mi = 8 reflectors per user for data communications offers 9 and 42 dB gain *vs*. one IRS M = Mi = 8 and without IRS [29].

Funding Statement: The authors received no specific funding for this study.

Conflicts of Interest: The authors declare that they have no conflicts of interest to report regarding the present study.

References

[1] E. Basar, M. Renzo, J. Rosny, M. Debbah, M. S. Alouini *et al.,* "Wireless communications through reconfigurable intelligent surfaces," *IEEE Access*, vol. 7, no. 2, pp. 116753–116773, 2019.

[2] H. Zhang, B. Di, L. Song and Z. Han, "Reconfigurable intelligent surfaces assisted communications with limited phase shifts: How many phase shifts are enough?," *IEEE Transactions on Vehicular Technology*, vol. 69, no. 4, pp. 4498–4502, 2020.

[3] M. Renzo, "6G wireless: Wireless networks empowered by reconfigurable intelligent surfaces," in *25th Asia-Pacific Conf. on Communications (APCC)*, vol. 1, no. 1, pp. 12–13, 2019.

[4] E. Basar, "Reconfigurable intelligent surface-based index modulation: A new beyond MIMO paradigm for 6G," *IEEE Transactions on Communications*, vol. 68, no.5, pp. 3187–3196, 2020.

[5] Q. Wu and R. Zhang, "Towards smart and reconfigurable environment: Intelligent reflecting surface aided wireless network," *IEEE Communications Magazine*, vol. 58, no. 1, pp. 106–112, 2020.

[6] C. Huang, A. Zappone, G. Alexandropoulos, M. Debbah and C. Yuen, "Reconfigurable intelligent surfaces for energy efficiency in wireless communication," *IEEE Transactions on Wireless Communications*, vol. 18, no. 8, pp. 4157–4170, 2019.

[7] G. C. Alexandropoulos and E. Vlachos, "A hardware architecture for reconfigurable intelligent surfaces with minimal active elements for explicit channel estimation," in *ICASSP 2020-2020 IEEE Int. Conf. on Acoustics, Speech and Signal Processing (ICASSP)*, vol. 1, no.1, pp. 9175–9179, 2020.

[8] H. Guo, Y. Liang, J. Chen and E. Larsson, "Weighted sum-rate maximization for reconfigurable intelligent surface aided wireless networks," *IEEE Transactions on Wireless Communications*, vol. 19, no. 5, pp. 3064–3076, 2020.

[9] V. Thirumavalavan and T. Jayaraman, "BER analysis of reconfigurable intelligent surface assisted downlink power domain NOMA system," in *2020 Int. Conf. on COMmunication Systems and NETworkS (COMSNETS)*, vol. 1, no. 2, pp. 519–522, 2020.

[10] C. Pradhan, A. Li, L. Song, B. Vucetic and Y. Li, "Hybrid precoding design for reconfigurable intelligent surface aided mmwave communication systems," *IEEE Wireless Communications Letters*, vol. 9, no. 7, pp. 1041–1045, 2020.

[11] K. Ying, Z. Gao, S. Lyu, Y. Wu, H. Wang *et al.,* "GMD-Based hybrid beamforming for large reconfigurable intelligent surface assisted millimeter-wave massive MIMO," *IEEE Access*, vol. 8, no. 2, pp. 19530–19539, 2020.

[12] L. Yang, W. Guo and I. Ansari, "Mixed dual-hop FSO-RF communication systems through reconfigurable intelligent surface," *IEEE Communications Letters*, vol. 24, no. 7, pp. 1558–1562, 2020.

[13] B. Di, H. Zhang, L. Li, L. Song, Y. Li *et al.,* "Practical hybrid beamforming with finite-resolution phase shifters for reconfigurable intelligent surface based multi-user communications," *IEEE Transactions on Vehicular Technology*, vol. 69, no. 4, pp. 4565–4570, 2020.

[14] Q. Nadeem, A. Kammoun, A. Chaaban, M. Debbah and M. Alouini, "Asymptotic max-min SINR analysis of reconfigurable intelligent surface assisted MISO systems," *IEEE Transactions on Wireless Communications*, vol. 19, no. 12, pp. 7748–7764, 2020.

[15] W. Zhao, G. Wang, S. Atapattu, T. Tsiftsis and C. Tellambura, "Is backscatter link stronger than direct link in reconfigurable intelligent surface-assisted system?" *IEEE Communications Letters*, vol. 24, no. 6, pp. 1342–1346, 2020.

[16] S. Li, B. Duo, X. Yuan, Y. Liang and M. Renzo, "Reconfigurable intelligent surface assisted UAV communication: Joint trajectory design and passive beamforming," *IEEE Wireless Communications Letters*, vol. 9, no. 5, pp. 716–720, 2020.

[17] L. Dai, B. Wang, M. Wang, X. Yang, J. Tan *et al.,* "Reconfigurable intelligent surface-based wireless communications: Antenna design, prototyping and experimental results," *IEEE Access*, vol. 8, no. 3, pp. 45913–45923, 2020.

[18] S. Hua and Y. Shi, "Reconfigurable intelligent surface for green edge inference in machine learning," in *2019 IEEE Globecom Workshops (GC Wkshps)*, vol. 2, no. 3, pp. 10–15, 2019.

[19] C. Huang, G. Alexandropoulos, C. Yuen and M. Debbah, "Indoor signal focusing with deep learning designed reconfigurable intelligent surfaces," in *IEEE 20th Int. Workshop on Signal Processing Advances in Wireless Communications (SPAWC)*, vol. 3, no. 4, pp. 11–14, 2019.

[20] B. Yin, S. W. Zhou, S. W. Zhang, K. Gu and F. Yu, "On efficient processing of continuous reverse skyline queries in wireless sensor networks," *KSII Transactions on Internet and Information Systems*, vol. 11, no. 4, pp. 1931–1953, 2017.

[21] J. M. Zhang, K. Yang, L. Y. Xiang, Y. S. Luo, B. Xiong *et al.,* "A Self-adaptive regression-based multivariate data compression scheme with error bound in wireless sensor networks," *International Journal of Distributed Sensor Networks*, vol. 9, no. 3, pp. 913497, 2013.

[22] J. Wang, C. Ju, Y. Gao, A. K. Sangaiah and G. J. Kim, "A PSO based energy efficient coverage control algorithm for wireless sensor networks," *Computers Materials & Continua*, vol. 56, no. 3, pp. 433–446, 2018.

[23] J. Wang, X. J. Gu, W. Liu, A. K. Sangaiah and H. J. Kim, "An empower hamilton loop based data collection algorithm with mobile agent for WSNs," *Human-centric Computing and Information Sciences*, vol. 9, no. 1, pp. 1–14, 2019.

[24] J. Wang, Y. Gao, C. Zhou, S. Sherratt and L. Wang, "Optimal coverage multi-path scheduling scheme with multiple mobile sinks for WSNs," *Computers, Materials & Continua*, vol. 62, no. 2, pp. 695–711, 2020.

[25] J. Wang, Y. Gao, W. Liu, W. Wu and S. J. Lim, "An asynchronous clustering and mobile data gathering schema based on timer mechanism in wireless sensor networks," *Computers Materials & Continua*, vol. 58, no. 3, pp. 711–725, 2019.

[26] J. Wang, Y. Gao, X. Yin, F. Li and H. J. Kim, "An enhanced PEGASIS algorithm with mobile sink support for wireless sensor networks," *Wireless Communications and Mobile Computing*, 2018, https://doi.org/10.1155/2018/9472075.

[27] Q. Tang, K. Yang, P. Li, J. M. Zhang, Y. S. Luo *et al.,* "An energy efficient MCDS construction algorithm for wireless sensor networks," *EURASIP Journal on Wireless Communications and Networking*, 2012, https://doi.org/10.1186/1687-1499-2012-83.

[28] Z. Liao, J. Wang, S. Zhang, J. Cao and G. Min, "Minimizing movement for target coverage and network connectivity in mobile sensor networks," *IEEE Transactions on Parallel and Distributed Systems*, vol. 26, no. 7, pp. 1971–1983, 2014.

[29] R. Alhamad and H. Boujemaa, "Optimal harvesting and sensing durations for cognitive radio networks," *Signal Image Video Process*, vol. 14, no. 7, pp. 1397–1404, 2020.

[30] J. Proakis, "Digital communications," Mac Graw-Hill, 5th edition, 1221 Aveue of the Americas, New York, NY 10020, 2007.

[31] W. Wells, R. Anderson and J. Cell, "The distribution of the product of two central or non-central chi-square variates," *The Annals of Mathematical Statistics*, vol. 33, no. 3, pp. 1016–1020, 1962.

[32] X. Burr, A. Wei, J. Ben and D. Grace, "A general upper bound to evaluate packet error rate over quasi-static fading channels," *IEEE Trans. Wireless Communications*, vol. 10, no. 5, pp. 1373–1377, 2011.